Surface Topography: Metrology and Properties

The impact of surface slope and calculation resolution on the fractal dimension for fractures of steels after bending-torsion fatigue

To cite this article: Wojciech Macek 2022 *Surf. Topogr.: Metrol. Prop.* **10** 015030

IOP Publishing Surf. Topogr.: Metrol. Prop. **10** (2022) 015030 https://doi.org/10.1088/2051-672X/ac58ae

Surface Topography: Metrology and Properties

OPEN ACCESS

RECEIVED
21 December 2021

REVISED
18 February 2022

ACCEPTED FOR PUBLICATION
25 February 2022

PUBLISHED
8 March 2022

PAPER

The impact of surface slope and calculation resolution on the fractal dimension for fractures of steels after bending-torsion fatigue

Wojciech Macek
Gdańsk University of Technology, Faculty of Mechanical and Ship Technology, Gabriela Narutowicza11/12, 80-233 Gdańsk, Poland
E-mail: wojciech.macek@pg.edu.pl

Keywords: fractal dimension, fatigue, fracture, steel, bending-torsion

Abstract

The article presents the results of the fractal dimension measurements on the fatigue fracture surfaces of 10HNAP and S355J2 steels specimens after combined bending-torsion fatigue. For smooth and ring-notched specimens, three loading conditions were analyzed: (1) bending; (2) bending-torsion; and (3) torsion fatigue. Post-failure surface topography measurements were carried out on the entire fracture surfaces using an optical profilometer. The fractal dimension was computed with general slope and after removing them by leveling operation, as well as with two different resolutions. The analysis of the fractal dimension delineated by the enclosing boxes method (EBM) allowed to formulate guidelines that, in terms of further estimation of the method of failure, the optimum is extra-fine resolution without leveling.

1. Introduction

The ISO 3274, ISO 25178 [1, 2] and ISO 16610-21 [3] standards specify that the primary surface should not contain the nominal form of the component. It means that the microroughness must be removed along with the S filter and then, as needed, the L-filter which removes large-scale components or the F-operator with the form removal option, using levelling operations [4]. The metrologist should align the analised surface with the measurement axes as closely as possible. This is especially important in the widely developed field of material processing, where workpieces must be devoid of nominal forms for further metrological operations [5–7]. Filters for surface preparation are used in many branches of science, such as in biology [8], or geology and others [9]. But also, in particular, they are used in fatigue strength assessment, such as, for example, additively manufactured metallic structures [10]. In this study, the as-built surface around the whole specimen was analyzed and subjected to S- and F- filtration.

Fractals have an even wider range of application [11, 12]. In addition, the fractal dimension is an alternative to areas where traditional dimensioning may not be entirely sufficient [13–15]. Fractal dimension estimates the rank of geometric irregularity accounting for the objects, also for damaged structures [16, 17]. Bouchaud *et al* in 1990 published a paper [18] in which they analyzed specimens of aluminum alloy subjected to four different heat treatments and confirmed the fractal dimension could be used as a universal value in the case of fracture surfaces. Xing *et al.* [19] utilized the fractal dimension as a tool to suppose if the magnet is anisotropic. They used the SEM image of the fracture surface subjected to binarization, and then the box counting method.

The fractography and, inter alia, the crack initiation angle [20–23] suggest to the author a different approach of that recommended in surface metrology for topography parameters [24, 25]. Therefore, this work compares the results of the fractal dimension Df for different calculation methods, filtering and resolution settings [26, 27]. Following this strategy, the author has already published several works based on the fractal dimension Df without leveling with promising results [28–30]. These earlier analyzes also looked at fatigue fracture surfaces for the entire fracture areas. This work is an attempt to confirm the correctness of this approach.

In more detail, the present paper focuses on a better understanding of the fracture surface formation mechanisms of components made of steel subjected to fatigue loading, especially bending and torsion, because they are not completely understood; and the finding of the best way to calculate fractal dimensions to describe these surfaces. The methodology proposed in the paper can be directly adopted by the industry provided that

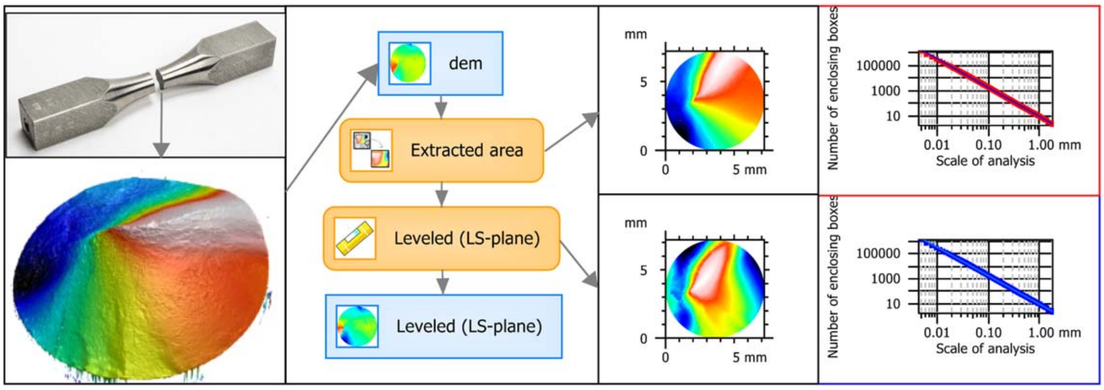

Figure 1. Research methodology scheme.

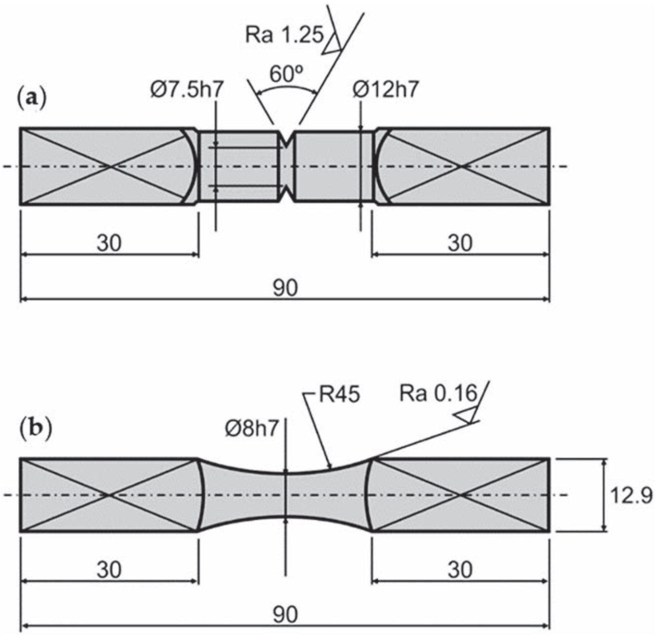

Figure 2. Specimens shapes and geometries: (a) 10HNAP steel; (b) S355J2 steel, dimensions in millimetres. Reproduced from [30]. CC BY 4.0.

there is an optical profiler and can be particularly useful to trace back the failure origin, as well as to provide important clues in forensic engineering.

2. Method

The following research chronology was used in this work: (2.1) fatigue tests for two types of specimens with different shapes; (2.2) surface topography measurements of fatigue fractures; and (2.3) evaluation of fractal dimension Df with different calculation methods and parameters. The research methodology is presented in figure 1.

2.1. Fatigue test

Both specimens geometries with a length of 90 mm used in the fatigue tests, V-notched round bar fabricated from 10HNAP, and smooth round bar made of S355J2 steel, are presented in figures 2(a) and (b) respectively. The main mechanical properties are listed in [29].

The fatigue campaign was performed with a stress ratio (R) equal to −1, considering both proportional stationary ergodic random (10HNAP) and non-proportional cyclic (S355J2) histories [29]. A total of six cases were tested for both type of specimens as well as three loading conditions: (1) bending; (2) bending-torsion; and (3) torsion fatigue.

2.2. Surface topography measurement

The fracture surfaces were measured and recorded using an Alicona IF G4 optical profilometer, see figure 3. This non-contact measuring system uses a white light source to project light beams onto a specimen's surface. Reflected light rays appear from the measured surface and are processed by a high-precision sensor. Measurements were made using the

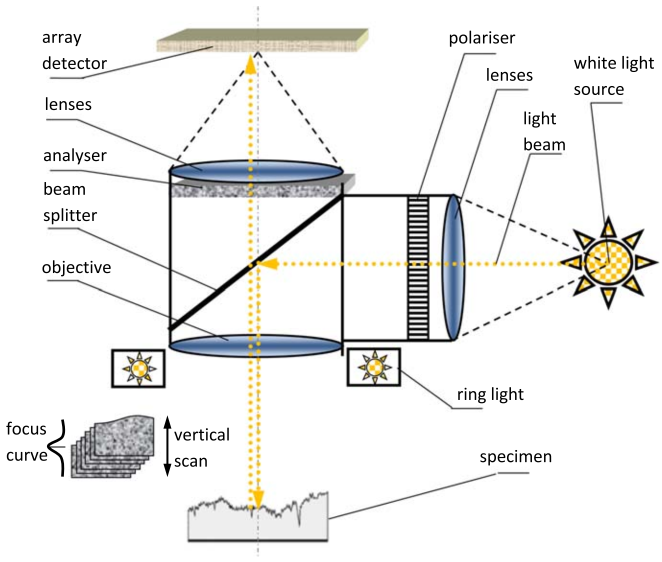

Figure 3. Scheme of the measurement using the Focus-variation method with alicona IF G4 profilometer.

focus variation microscopy (FVM) method [31] with 10x magnification, and additional measurements of the characteristic zones were made with 100 × magnification. FVM is an optical surface topography measurement technique in which the sharpness of a surface image at optimal focus positions in axial direction is used to establish the surface height. The main measurement parameters are listed in table 1.

The work also uses furrows analysis allowing the comparison of the micro-network for characteristic fracture zones. The study supplies the mean depth of the furrows, as well as the density of the furrows [32, 33]. Additionally, SEM pictures were made using the PFIB-SEM technique to obtain a cross-section of the post-failure of a 10HNAP steel specimen. Cross-section and pictures were taken with a SEM-PFIB FEI Helios microscope [34, 35].

Table 1. Alicona G4 profilometer main parameters used during the measurement.

Parameter	Value	
Magnification	10×	100×
Vertical resolution	79.62 nm	4.77 nm
Lateral resolution	3.91 μm	1.47 μm
Number of images	9 rows × 7 columns	13 rows × 10 columns
Exposure time	178 μs	429 μs
Contrast	0.53	0.70

2.3. Fractal dimension calculation

An analysis of the fractal dimension Df of the fracture surfaces was conducted using MountainsMap 9 software [36–38]. Height maps in the six analyzed fractures have been subjected to circular extract the area function, with a radius of 3.6 mm, to extract the region of interest (ROI). The extraction of the ROI is necessary to exclude from the following computations the effect of topographical features that are related to measurement discontinuities and faults occurring at the edges.

The analyzed surfaces were checked for the use of leveling to remove the general slope. Applied leveling method was least squares plane (LSPL) [39, 40]. LSPL is the mathematical model in disposition to best fit an actual surface, represented by a cloud of points. Least squares corresponds to the L2-norm (it is the shortest distance to from one point to another) as they minimize quadratic deviations. The method of leveling is presented in figure A1 (appendix) for the differences between extracted and leveled (LS-plane) surfaces. It is subtracted a surface from the selected extracted and leveled (LS-plane) surfaces. Leveling also causes further changes in the surface geometry, such as changing the position of the lowest and highest points of the fracture planes, as presented in the appendix (see figure A2).

The surface topographies were also checked for resolution influence. While partitioning of the surface, they have kept the track of number of iterations that take place. The resolution of the graph determines the number of iterations, and correspondingly, for ‘coarse resolutions’ it is 15 data points and for ‘Extra-fine resolution’ it is 96 data points. The data used to calculate the fractal dimension (Df), based on the enclosing boxes method (EBM), are detailed shown in figure 4 [41–43]. In the figure, the plots into the axes specified by number of enclosing boxes and scale of analysis for figures 4(a) and (b) are outlined, as well as the same data using a base 10 logarithmic scale for figures 4(c) and (d). The EBM divides the area into smaller sections with a width ε and calculates the field Aε of all fields covering the entire area. This is an iterative procedure in which the width of the field is changed to plot $\ln(A\varepsilon)/\ln(\varepsilon)$ (see figures 4(c) and (d)). To estimate the fractal dimension Df, a line is fitted using the least squares method. The absolute value of the slope of the fitted line is the estimation of the fractal dimension Df.

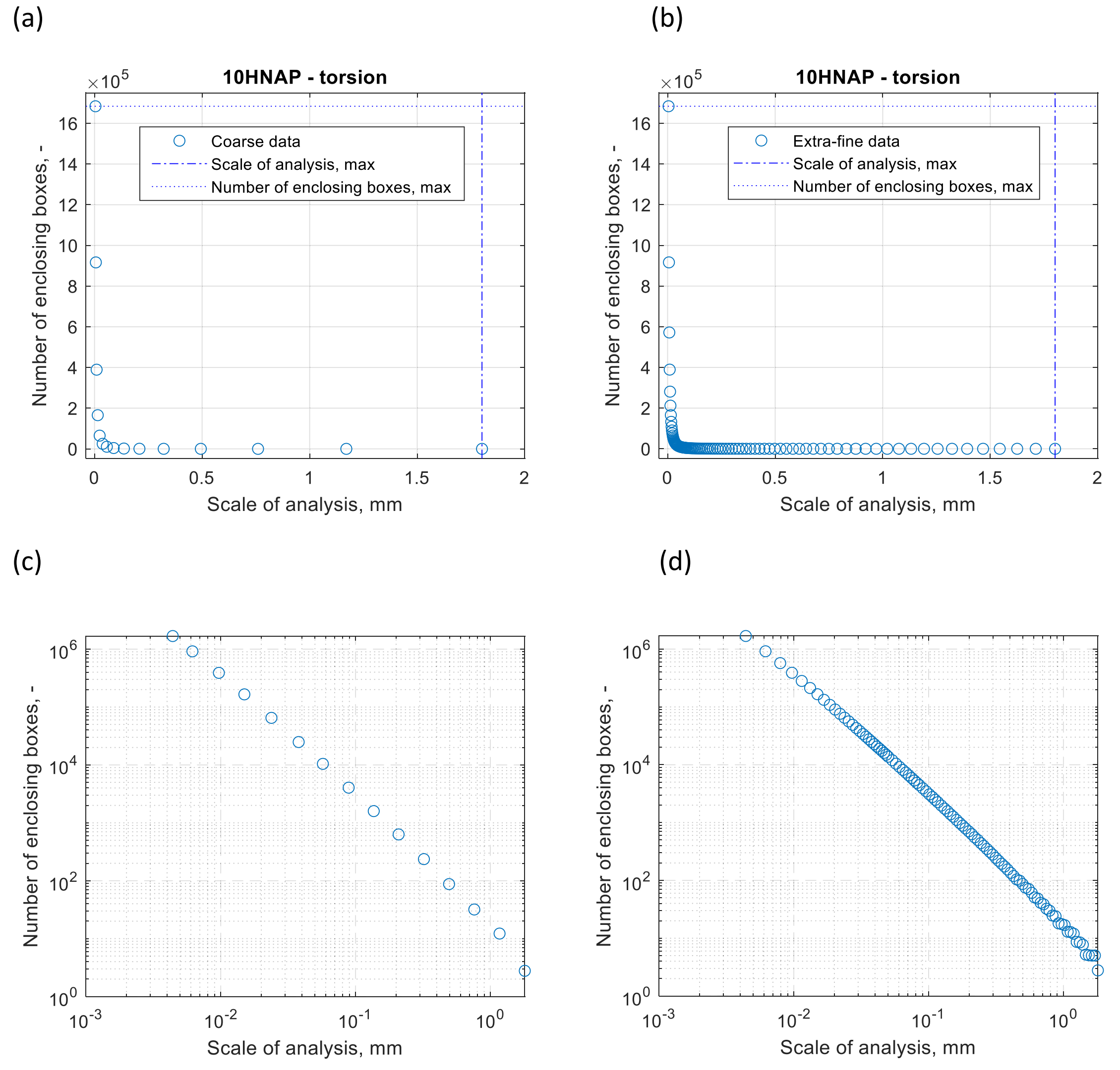

Figure 4. Fractal dimension Df data obtained using individual parameters for the 10 hnap specimen after torsion fatigue.

The graph of the calculated volume (for surfaces) is drawn as a function of the scale. A logarithmic scale is used for the axes, but the values of the scale markers are given as dimensional units.

In this work, the fractal dimension Df was also calculated using the morphological envelopes method [44], described later, for comparative purposes.

3. Results

Each graphs presented in figure 5 shows accordingly (starting from the top left corner): the 3D view of the fracture with extrated area selected; the 2D photo simulation with extracted area marked. Moreover, pseudo-color views of the extracted area (original and leveled) for each of them and the fractal dimension plots (coarse and extra-fine resolutions) with coefficients of correlation (R^2) computed by the enclosing boxes method. There are six sets of graphs for all analyzed cases.

On the example of sample in figure 5(a) (on both scales) it can be seen that the leveling operation had almost no effect on the difference in height of the lowest and highest point on the fracture surface. This situation also resulted in the same results of the fractal dimension Df (before and after leveling). On the other hand, the change of resolutions significantly influenced the fractal dimension Df (increase by 0.85% for extra-fine resolution).

For specimen 10HNAP bending-torsion (see figure 5(b)), the results of the fractal dimension Df for all calculation options are on a similar level (the ratio of the maximum and minimum Df values is 0.13%). The surface of this fracture is characterized by large pit and valley, but in a plane almost perfectly perpendicular to the *z*-axis due to the effect of the ring-notched shape of specimen.

10HNAP torsion (figure 5(c)), similarly to 10HNAP bending (figure 5(a)), the fractal dimension Df increased (by 0.41%) for extra-fine resolution, and the leveling did not affect the results almost at all.

In the case of S355J2 bending (see figure 5(d)), due to the slight change in plane slope after the leveling operation (as for figures 5(a) and (c)), only resolutions significantly influenced the result of Df (1.06% in favor of extra-fine resolution).

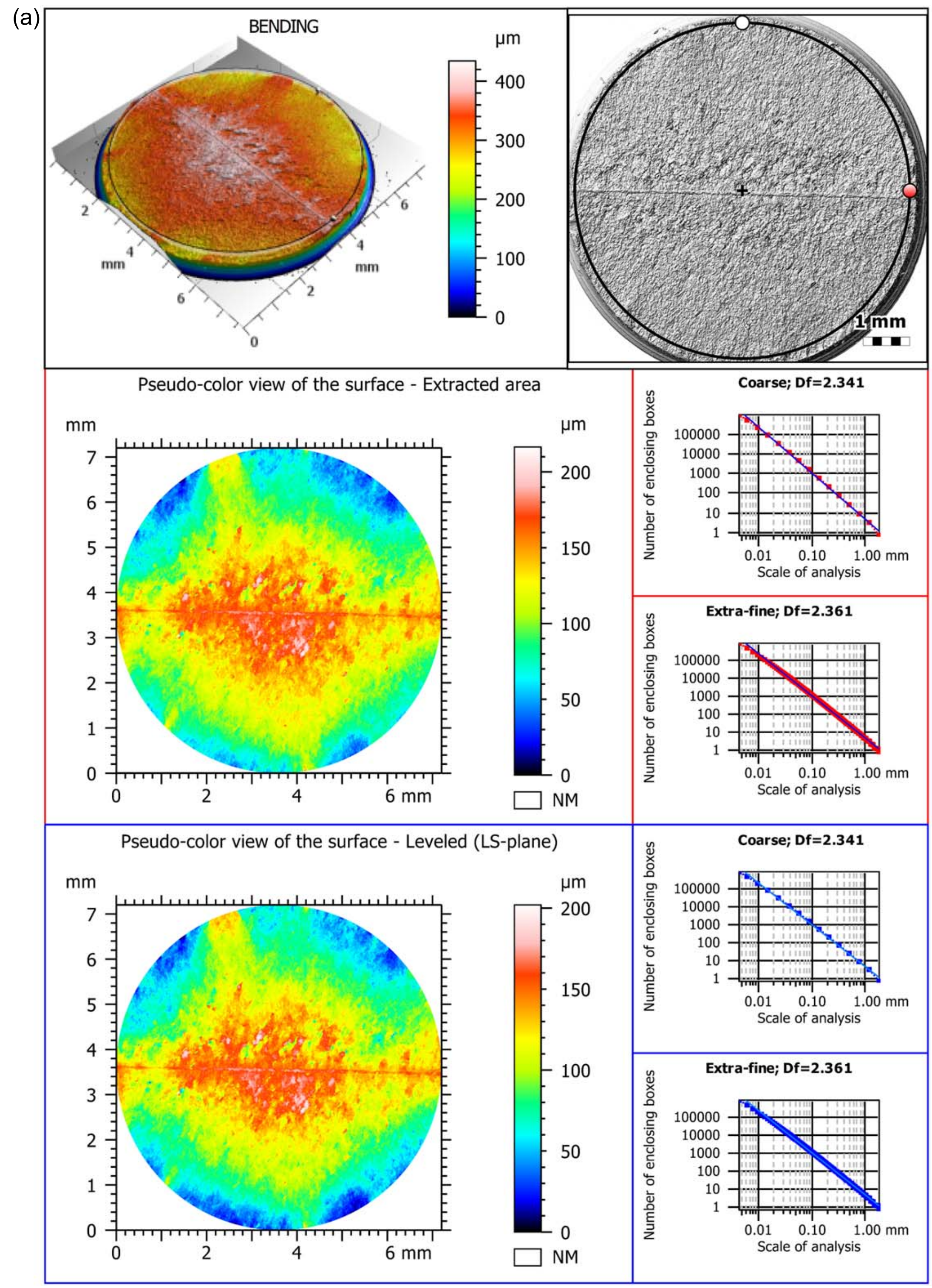

Figure 5. Original and extracted fracture surfaces with fractal dimension Df results: (a)–(c) 10HNAP steel specimens; and (d)–(f) S355J2 steels specimens.

An opposite situation occurs for the S355J2 bending-torsion fatigue fracture surface, where leveling, in turn, has a large impact on the result, while resolution is negligible. The increase in Df by 1.32% after leveling is due to the large slope change for this area of the fatigue fracture.

For the last analyzed case, which is the S355J2 torsion, a cascade arrangement of the fracture plane can be noticed, which generates a significant influence of leveling on its shape. This is reflected in a very high increase in the value of the fractal dimension Df, amounting to 4.10%.

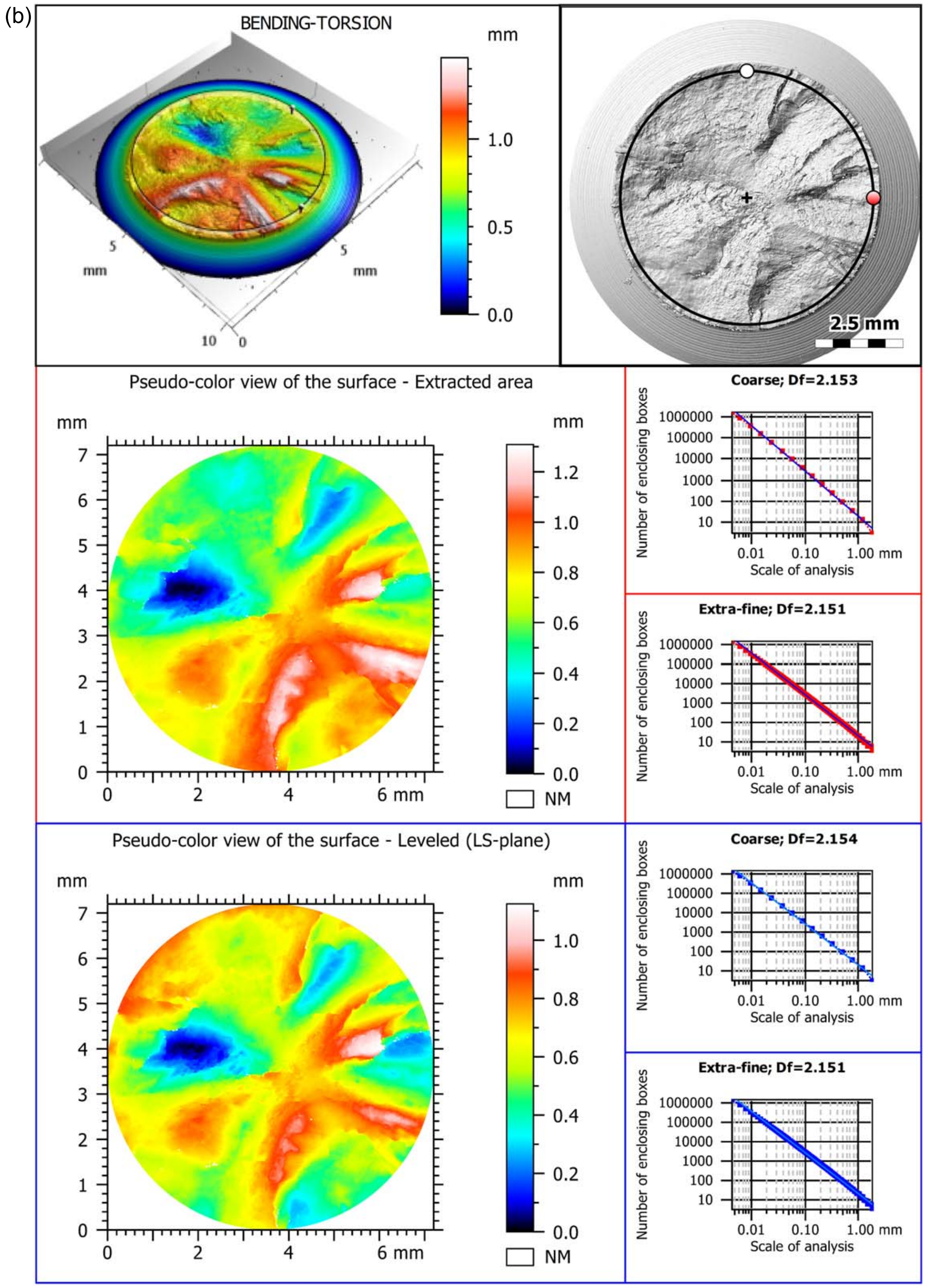

Figure 5. (Continued.)

4. Discussion

4.1. Distribution of fractal dimension values

All the results of the fractal dimension Df for six investigated specimens and four considered options for its calculation by the EBM are shown in figure 6.

As for the value of the fractal dimension Df, for both types of samples they were arranged in ascending order: bending-torsion, torsion, bending. This relationship was maintained for all calculation parameters. The exception is S355J2 torsion, which for both leveled cases, swapped with S355J2 bending. Apart from the case mentioned, all the samples had a relatively small scatter of values between the calculation methods. The exception mentioned (S355J2 torsion) had differences in the Df values from 2.219 to 2.310.

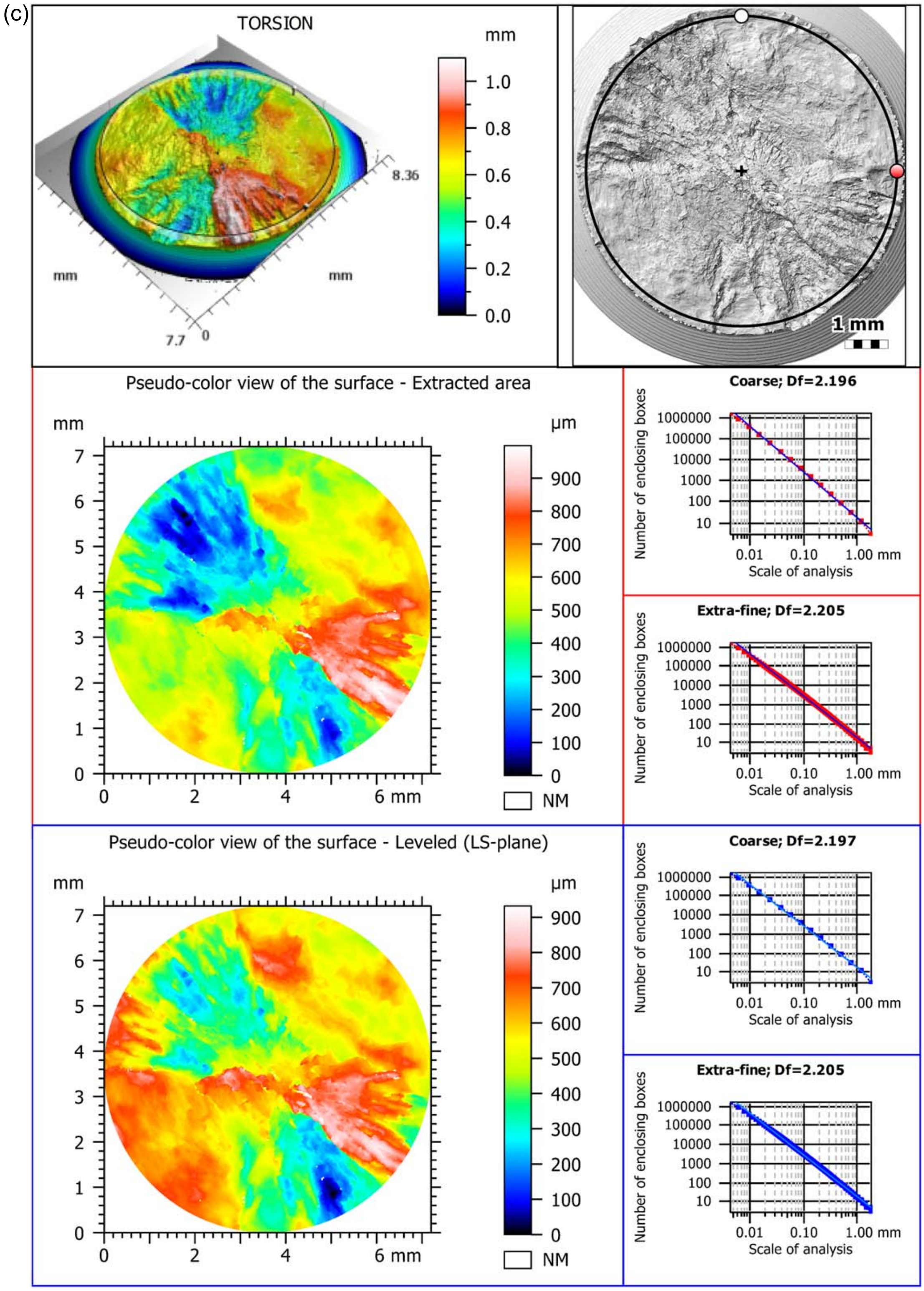

Figure 5. (Continued.)

Slope and coefficient of determination R^2 are calculated for two regression lines, one connecting the points to the left of the graph, the other connecting the points to the right (see figure 7). This makes it possible to analyze multi-fractal curves with two different slopes depending on the scales in the analysis. The fractal dimension Df is determined with a greater R^2 value. Figure 7 shows exemplary results for which R^2 (from slope (1)) is greater and it indicates the value of Df (absolute value).

For the curves with smaller number of points, the coefficient of determination R^2 is slighter than ones with higher numbers of points, which was confirmed by the results presented in figure 8. The best fit was noted for the sample S355J2 (BT), of course with

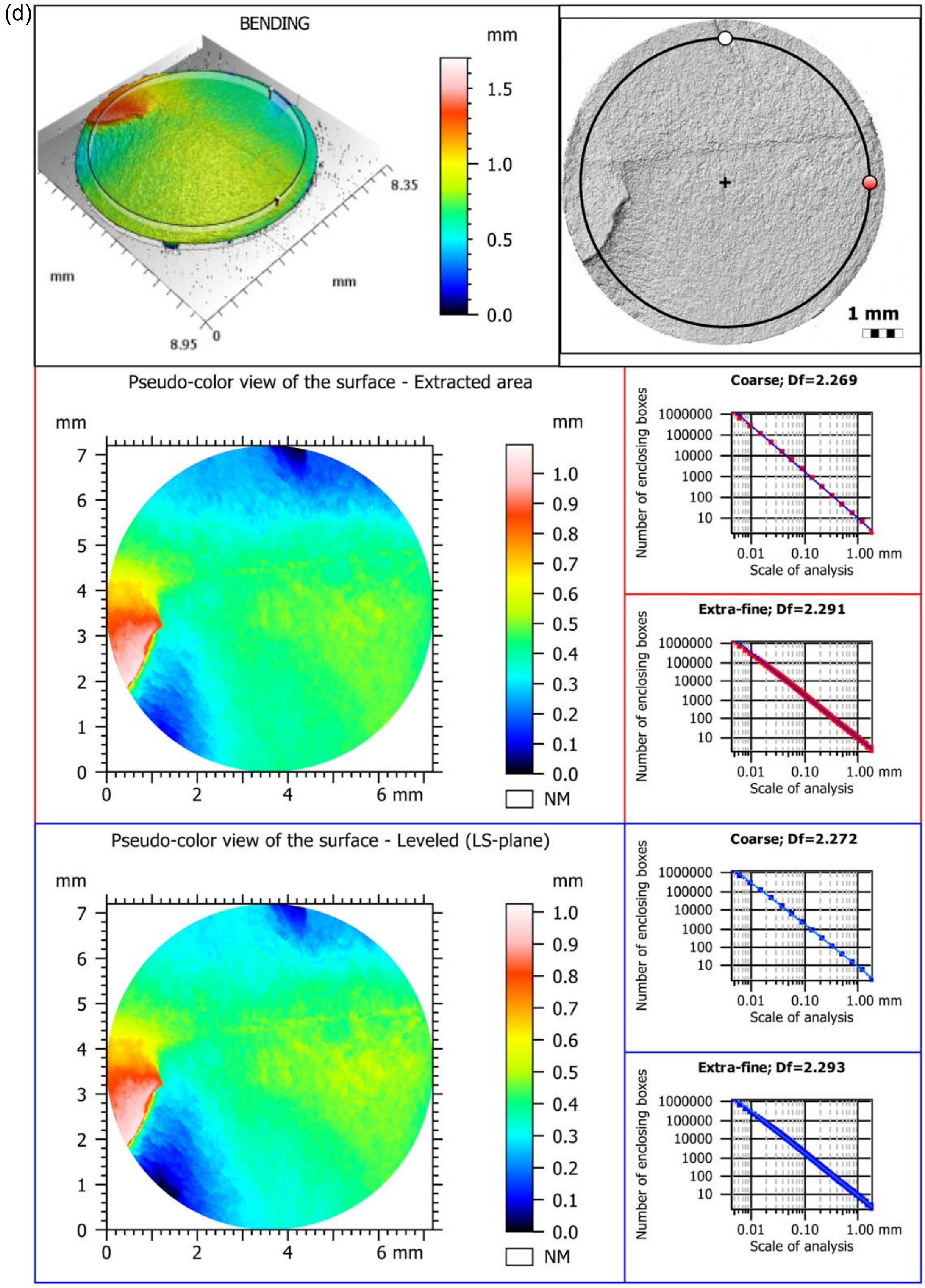

Figure 5. (Continued.)

extra-fine resolutions. In contrast, R^2 was the least for 10HNAP (T) when coarse resolutions were used.

4.2. Comparison of the fractal dimension determined by the enclosing boxes and morphological envelopes method

The recommendations of the standards and the software producer state that the enclosing boxes method for the fractal dimension must be applied on the primary profile or surface. This means that the surface must be prepared for the analysis: the small-scale components (S-filter) must be removed and the large-scale components (L-filter) too, using a leveling operation. Thus, it is very important that this study is applied on a leveled surface. After the leveling, the angle does not have any impact anymore. This is also true for all fractal analysis

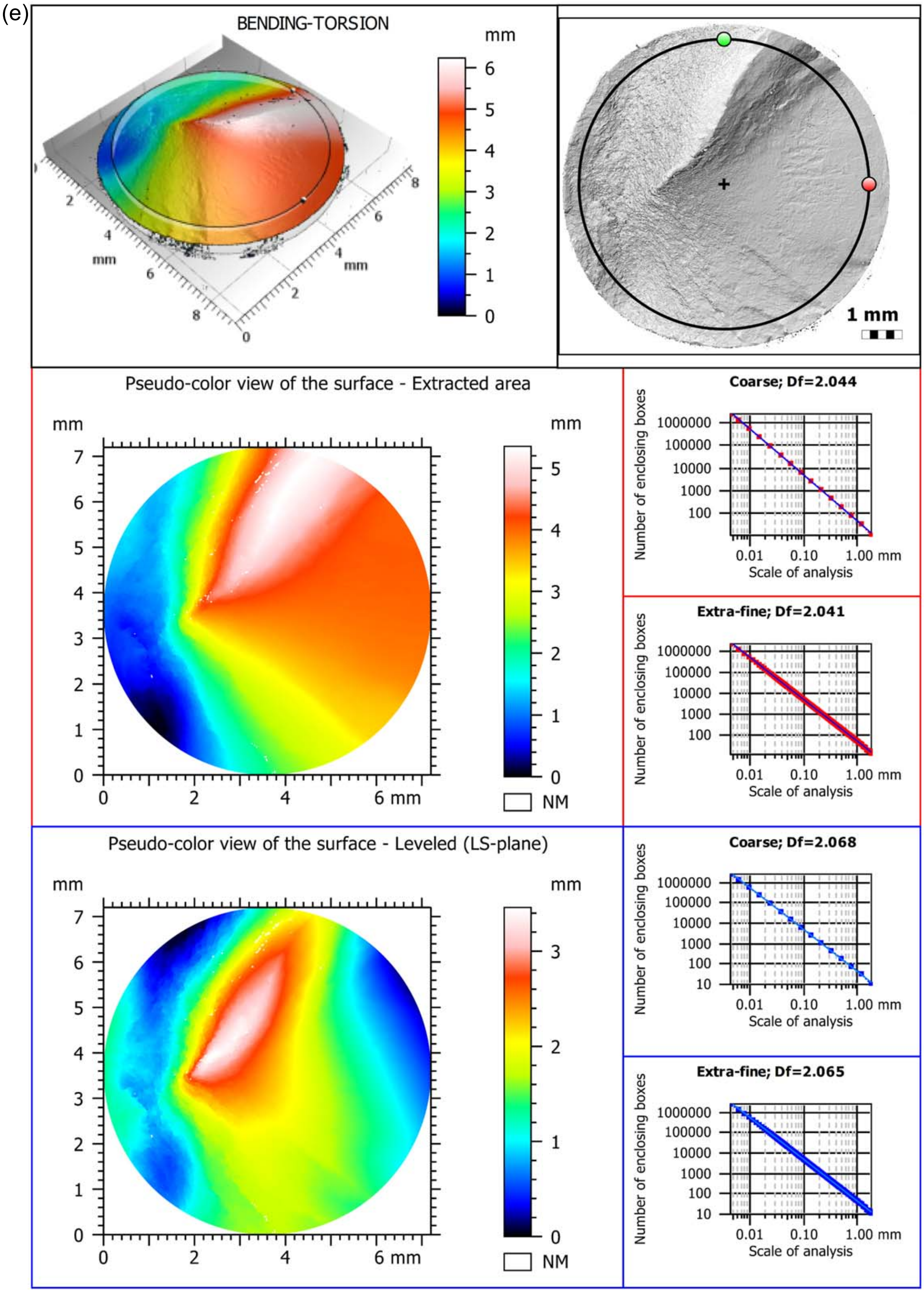

Figure 5. (Continued.)

methods, not only the enclosing boxes. However, in the case of analyzes of the surface of fatigue fractures, the inclinations planes are of interest.

This subsection compares the values of the fractal dimension Df determined by the Morphological envelopes method. For this method the upper and lower envelopes are calculated by morphological opening and closing using a structuring element which is a horizontal line-segment of length ε. Next the volume, $V\varepsilon$ enclosed between the elements is calculated. This procedure is iterated with structuring elements of different lengths to build a graph $\ln(V\varepsilon)/\ln(\varepsilon)$.

As part of the comparison, the fractal dimension was calculated using the morphological envelopes method, and the results are shown in figure 9. Due to

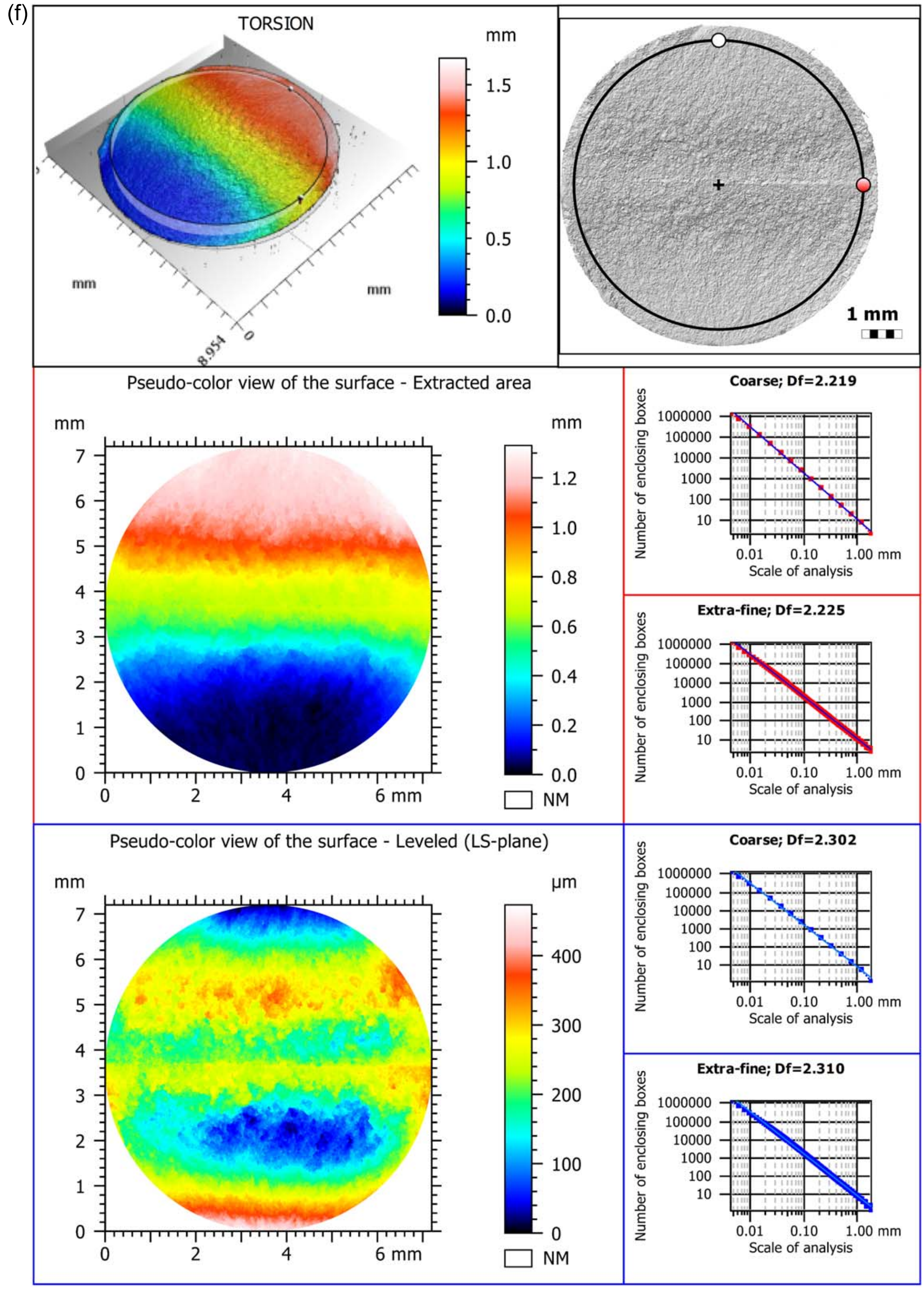

Figure 5. (Continued.)

the time-consuming nature of this calculation, the Coarse resolution was used for this method.

The results obtained from the morphological envelopes method with coarse resolution were compared with the results of the enclosing boxes method with extra-fine resolutions, as the best option for describing fatigue fractures (see figures 10 and 11). Both methods were used for the extracted area, without the leveling operation. Figure 10 shows the bar graph of the Df results grouped by material and loading case obtained by two methods. Figure 11 shows the correlation between the fractal dimension Df obtained for all tested cases for both calculated method. The fit residuals, as a bar plot, are also displayed in the bottom part of the same figure. As can be seen, both methods showed a fairly good fit, reaching

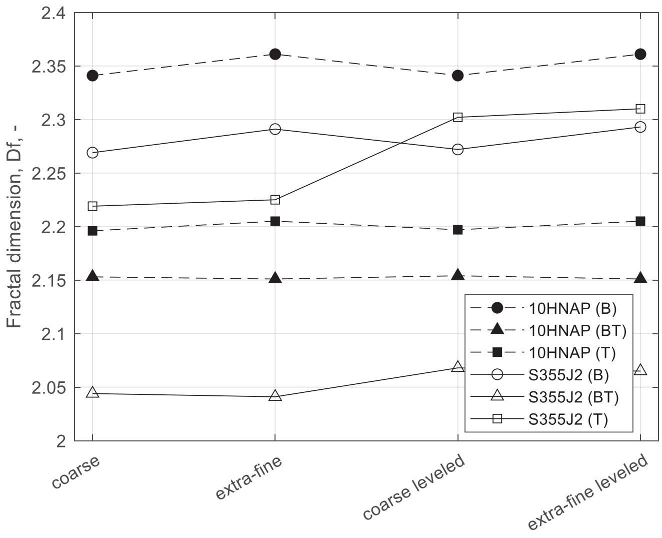

Figure 6. Results of fracture surface fractal dimension Df calculations grouped by specimens type.

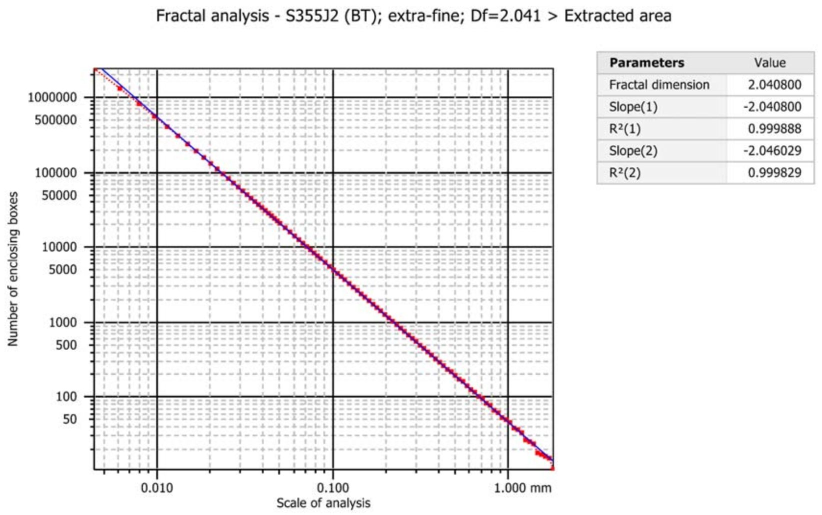

Fractal analysis - S355J2 (BT); extra-fine; Df=2.041 > Extracted area

Parameters	Value
Fractal dimension	2.040800
Slope(1)	-2.040800
R²(1)	0.999888
Slope(2)	-2.046029
R²(2)	0.999829

Figure 7. Fractal analysis for S355J2 (BT) fracture surface with selected parameters, for enclosing boxes method.

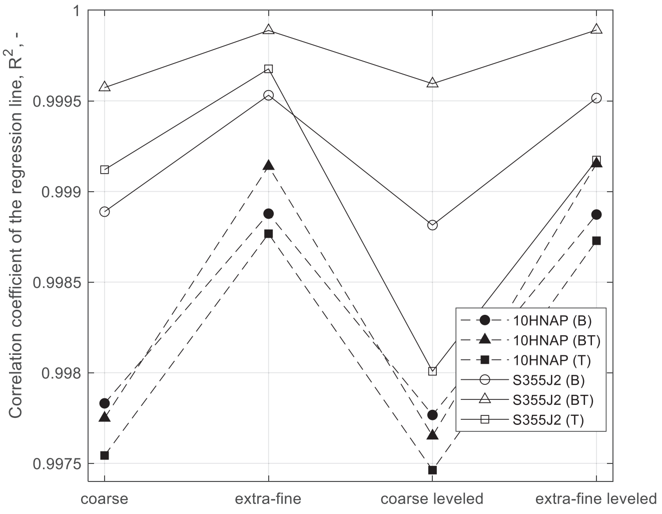

Figure 8. Results of correlation coefficient of the regression line R^2 calculations grouped by specimens type.

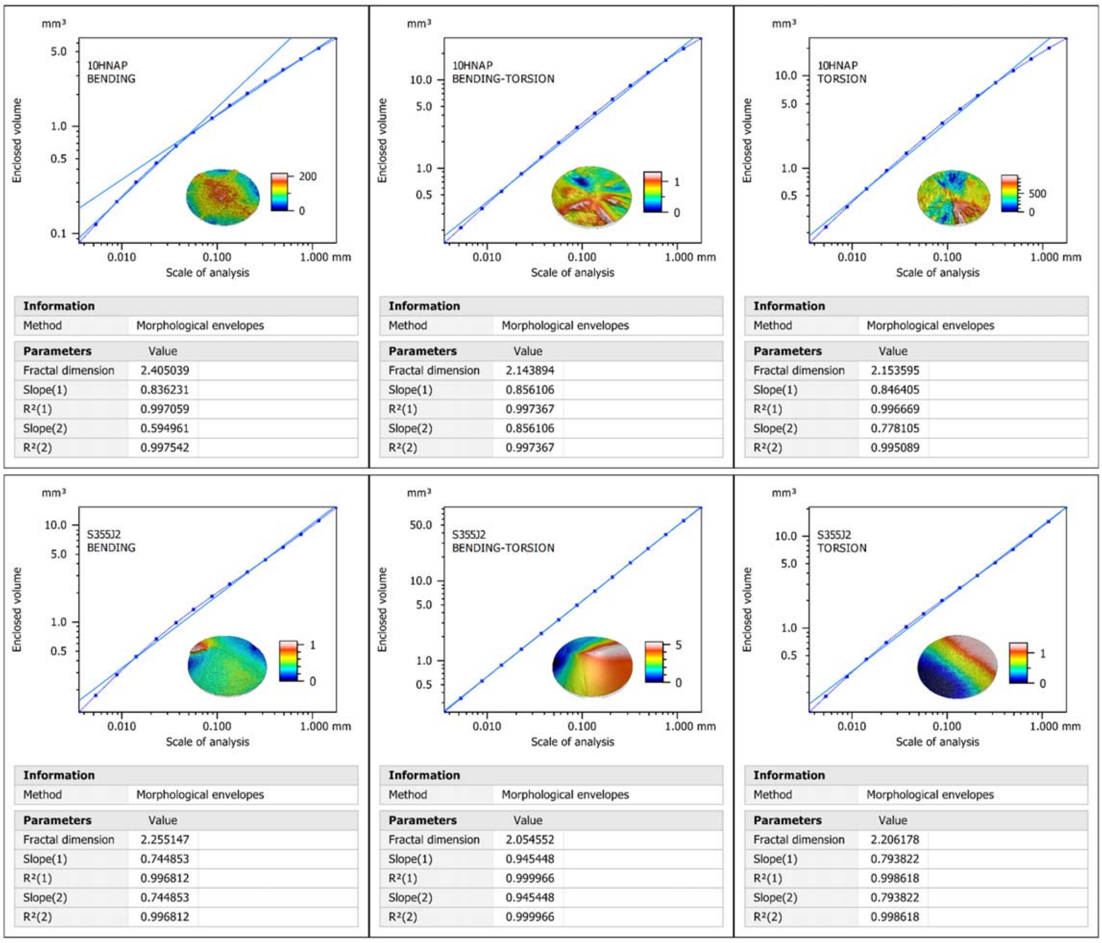

10HNAP BENDING

Information	
Method	Morphological envelopes

Parameters	Value
Fractal dimension	2.405039
Slope(1)	0.836231
R²(1)	0.997059
Slope(2)	0.594961
R²(2)	0.997542

10HNAP BENDING-TORSION

Information	
Method	Morphological envelopes

Parameters	Value
Fractal dimension	2.143894
Slope(1)	0.856106
R²(1)	0.997367
Slope(2)	0.856106
R²(2)	0.997367

10HNAP TORSION

Information	
Method	Morphological envelopes

Parameters	Value
Fractal dimension	2.153595
Slope(1)	0.846405
R²(1)	0.996669
Slope(2)	0.778105
R²(2)	0.995089

S355J2 BENDING

Information	
Method	Morphological envelopes

Parameters	Value
Fractal dimension	2.255147
Slope(1)	0.744853
R²(1)	0.996812
Slope(2)	0.744853
R²(2)	0.996812

S355J2 BENDING-TORSION

Information	
Method	Morphological envelopes

Parameters	Value
Fractal dimension	2.054552
Slope(1)	0.945448
R²(1)	0.999966
Slope(2)	0.945448
R²(2)	0.999966

S355J2 TORSION

Information	
Method	Morphological envelopes

Parameters	Value
Fractal dimension	2.206178
Slope(1)	0.793822
R²(1)	0.998618
Slope(2)	0.793822
R²(2)	0.998618

Figure 9. Fractal dimension determined by morphological envelopes method of 10HNAP and S355J2 samples.

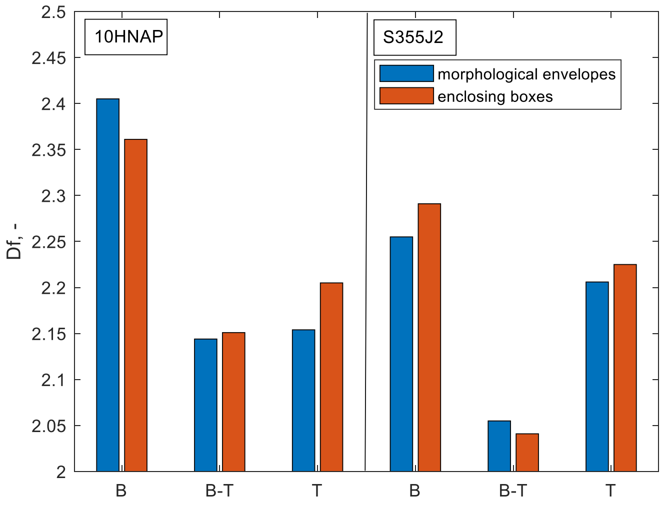

Figure 10. Bar graph for Df results grouped by material and loading case of two methods bars.

the coefficient of determination $R^2 = 0.9176$, for linear fitting.

4.3. The highest and lowest fractal dimension cases

Definitely the highest values of the fractal dimension Df = 2.361 were achieved for the 10HNAP bending case, and the lowest Df = 2.041 for S355J2 bending-torsion fatigue. These two extreme cases are magnified for the two fractures areas (propagation and rupture), and presented in figure 12. In figure 12, we also see a 2D graph showing contour lines of surface points lying at the same height level, dividing the surface into regularly spaced out horizontal slices. In the same figure, we also see the slope distribution in ROI, i.e. the

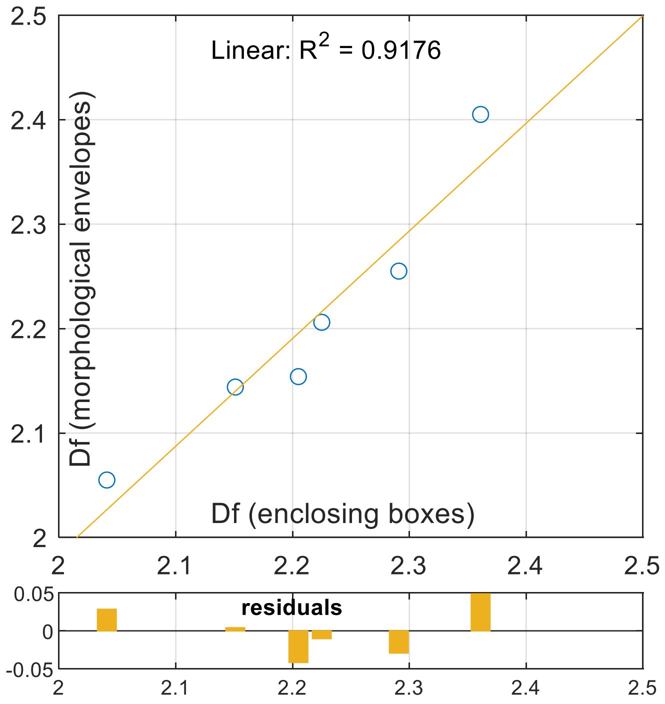

Figure 11. Fractal dimension Df calculated with morphological envelopes method versus Df obtained with enclosing boxes method.

slope analysis of all triangular tiles composing the surface.

For both extreme cases we see a high increase for the rupture area relative to the propagation. In the slope distribution plot we see the polar angle with the number of bins 90 and the width of each bin 1 degree. For the S355J2 bending-torsion loading case (D = 2.041), the angle distribution is more uniform than for the maximum Df case.

4.4. Fracture zones surface morphology

In figure 13, another 100 μm × 100 μm zoom was made for the same areas to provide detailed information on the pits and valleys geometry. The furrows analysis was also presented and the parameters describing the micro-valleys network were determined (see table 2).

In the case of S355J2 bending-torsion, in the propagation zone, larger grain size and elongation as well as directionality are evident. Figure 13 shows that, for the case of S355J2 bending-torsion loading (Df = 2.041), in the rupture zone, the valleys distribution is less uniform than for the case of maximum Df in the same zone. On the surface of this part of the fracture, the furrows are much deeper. In table 2, the results clearly indicate that the values of the maximum depth of furrows are smaller in the propagation zone than in the rupture zone and constitute their part expressed as a percentage, respectively 21.3% for 10HNAP and 35.2% for S355J2 steel.

Regarding the microstructure, the 10HNAP steel is a low-alloy structural steel consisting of a fine-grained ferritic-perlitic structure. In order to present it, additionally, micrographs of a 10HNAP microstructure after fatigue failure using PFIB-SEM technique were made. SEM pictures were taken for the cross-section of the surface and shown in figure 14. The cross-sectional surface was sliced by removing continuously a thin layer in the *Z*-axis direction with ion beam machining. Ferrite grains are visible as the brighter fields in the structure.

On the other hand, the S355J2 steel is a high-strength low-alloy steel composed of a ferrite-pearlite matrix with low pearlite [45].

5. Summary and conclusions

Finally, figure 15 shows boxplots for averages fractal dimension Df values grouped by EBM and also morphological envelopes method of calculations parameters. As can be seen, when averaging, both leveling and higher resolution increase the value of the fractal dimension Df. The densification of the measurement points increases the slope of the curve angle, which is reflected in a slightly higher value of the fractal dimension Df.

From the point of view of a surface metrologist, leveling and possibly other filters should be used for all surface cases, depending on the situation. On the other hand, from the point of view of the researcher of fracture mechanics, the optimal calculation option for the fractal Df dimension for EBM is extra-fine resolution, without leveling. The cracking mechanisms predispose, among others, the crack initiation angle, therefore the fracture surface slope should be kept for analysis. Additionally, using EBM is easier and faster to calculate fractal dimension Df than for example with the morphological envelopes method.

By establishing fractal dimension Df for bending-torsion fatigued specimens and analysing the

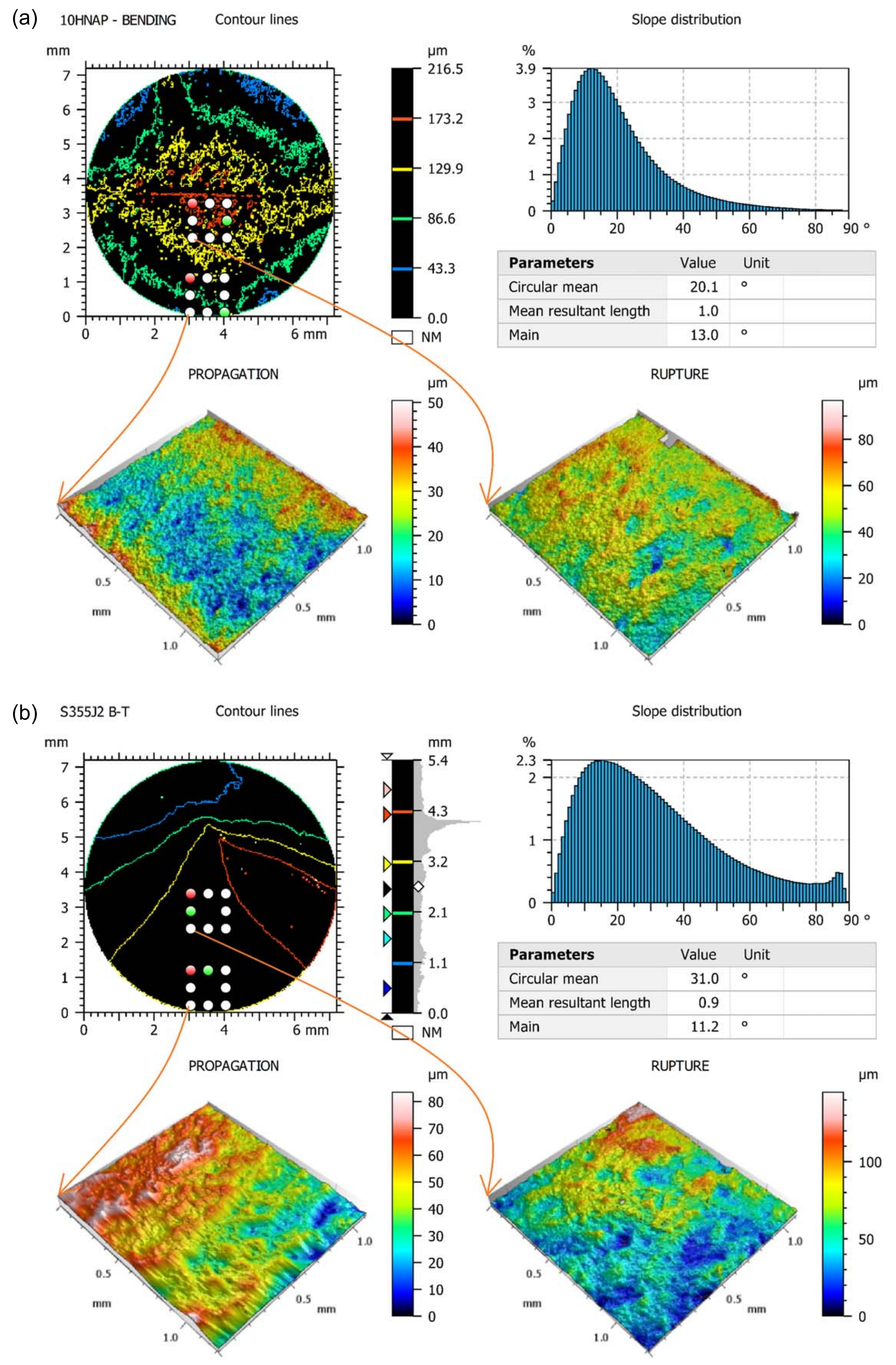

(a)

Parameters	Value	Unit
Circular mean	20.1	°
Mean resultant length	1.0	
Main	13.0	°

(b)

Parameters	Value	Unit
Circular mean	31.0	°
Mean resultant length	0.9	
Main	11.2	°

Figure 12. Extreme cases of fractal dimension Df showing the propagation and rupture areas for (a) 10HNAP bending (Df = 2.361) and (b) S355J2 bending-torsion loading (Df = 2.041).

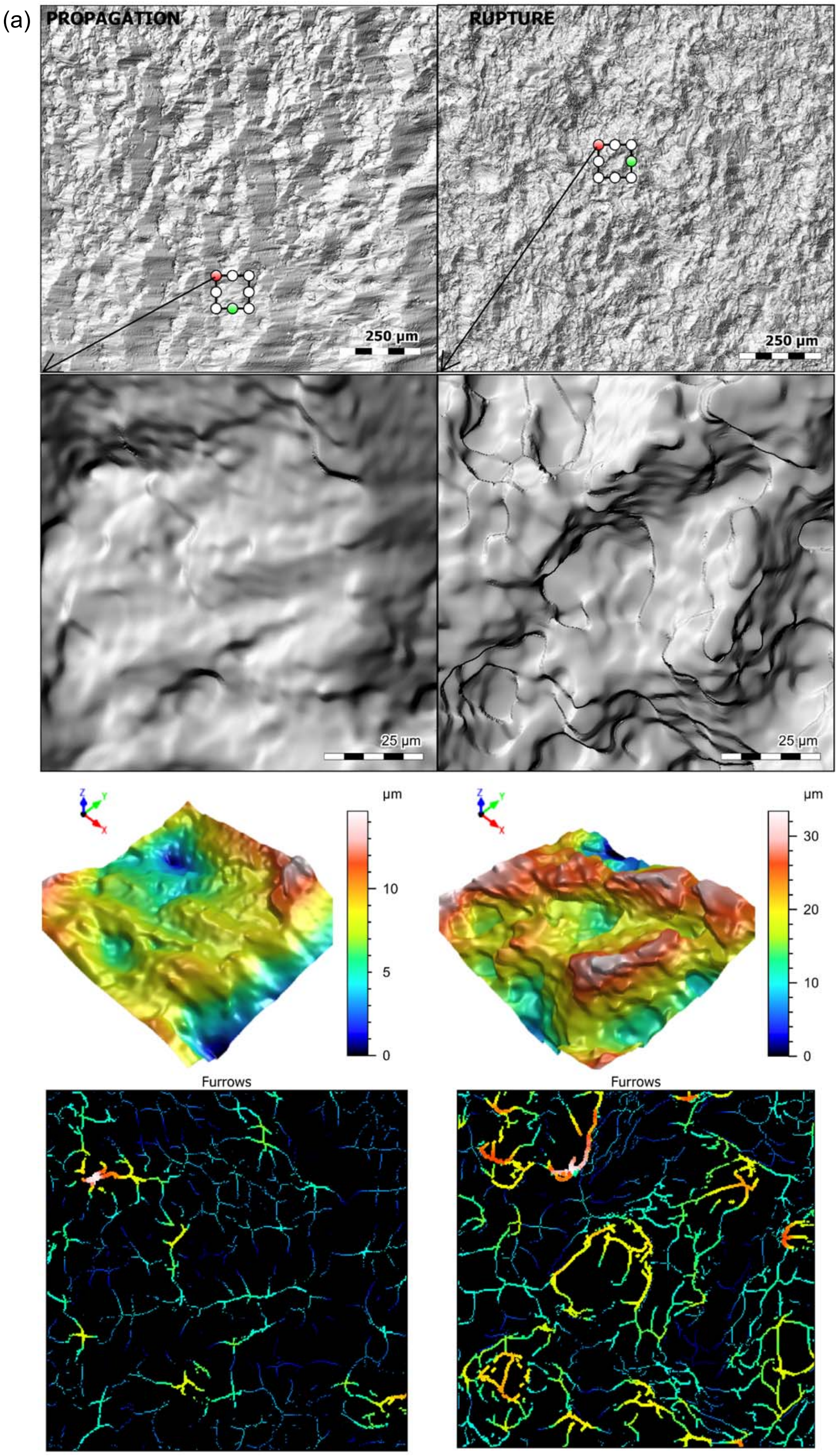

Figure 13. Extreme cases of fractal dimension Df (EBM) surfaces views with micro-valleys network for (a) 10HNAP bending (Df = 2.361) and (b) S355J2 bending-torsion loading (Df = 2.041).

fracture surface features, allows to indirectly identify the causes of the damage. The conclusions are as follows:

- leveling disturbed the order of results (bending-torsion, torsion, bending) and increased Df by 4.10% for the S355J2 torsion specimen. After

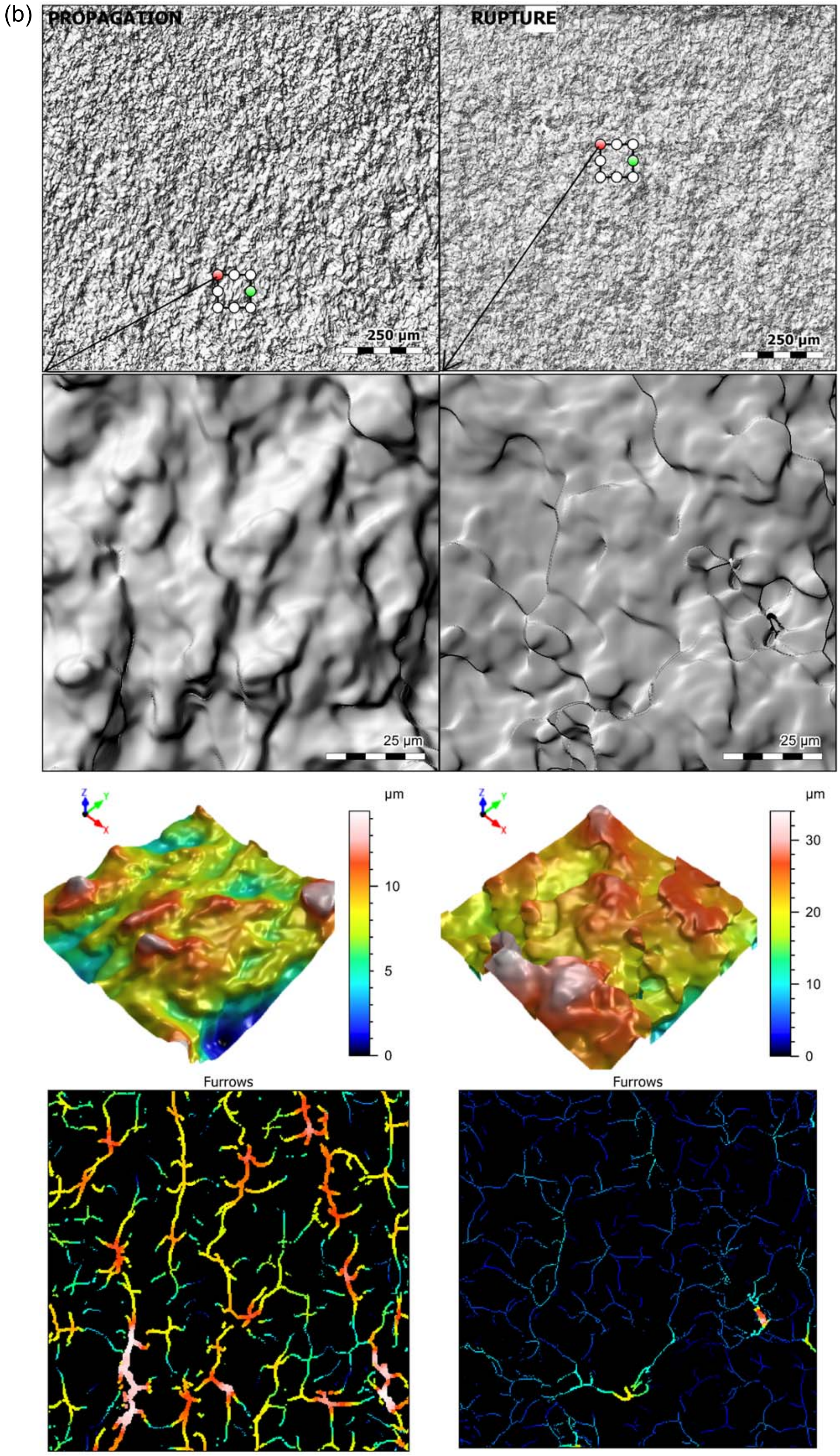

Figure 13. (Continued.)

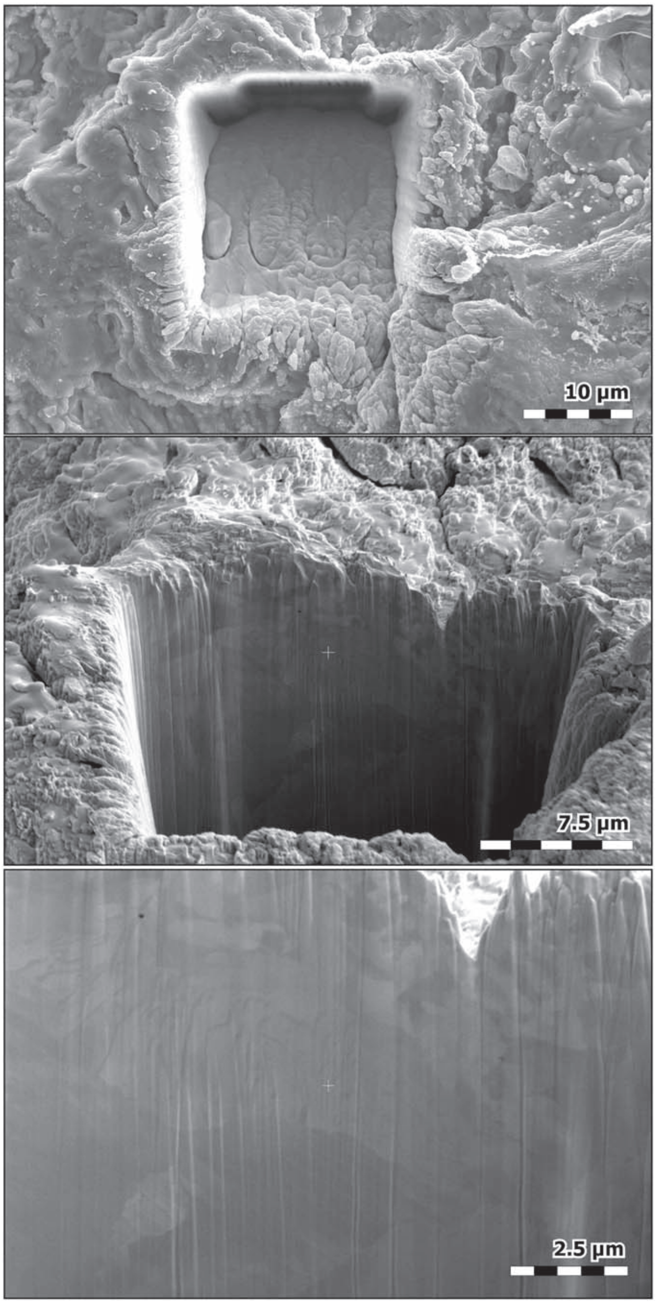

Figure 14. Cross-section obtained with a dual-beam FIB-SEM microscope for a 10HNAP steel fracture with a magnifications (respectively from the top) of 3500×; 6500×; 15000×.

Table 2. Furrows network parameters.

	10HNAP		S355J2		
Furrows parameter	propagation	Rupturę	propagation	rupture	Unit
Maximum depth of furrows	4.18	19.60	4.08	11.60	μm
Mean depth of furrows	2.07	3.43	0.99	3.84	μm
Mean density of furrows	1579	1835	1596	2458	cm/cm^2

leveling resulted in a large slope change for this surface of the fatigue fracture;

- resolutions significantly affected the result of Df (1.06% in favor of extra-fine resolution) for the S355J2 bending specimen because the densification of the measurement points increased the slope of the curve angle for fractal dimension Df;

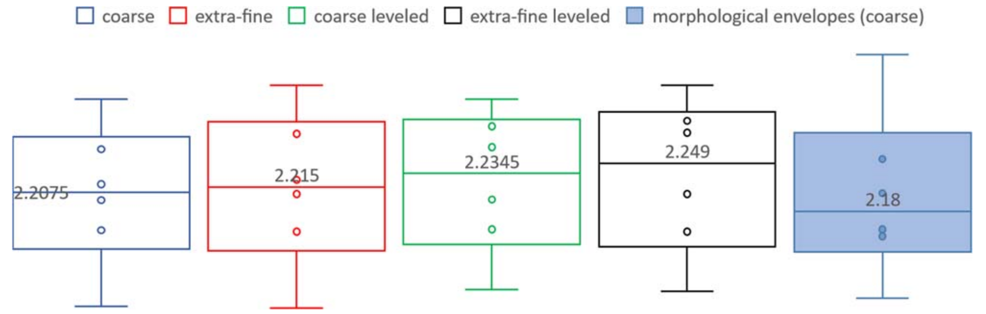

Figure 15. Boxplots for fractal dimension Df grouped by EBM and morphological envelopes method calculations parameters.

- In general, both leveling and higher resolution increased the value of the fractal dimension Df;
- the analysis of the propagation and rupture zones for fractures with extreme fractal dimension values showed that the high increase occurred in the rupture area;
- slope distribution showed for the S355J2 bending-torsion loading case (Df = 2.041) that the angle distribution is more uniform than that for the maximum Df case;
- also for the case of S355J2 bending-torsion loading (Df = 2.041), in the rupture zone, the valleys distribution is less uniform and has deeper furrows;
- maximum depth of furrows are greater in the rupture zone than in the propagation zone, i.e. about 469% and 284% for 10HNAP bending and S355J2 bending-torsion, respectively;
- for the S355J2 bending-torsion in the propagation area, there is also a clear tendency to elongation and larger grain size as well as directionality;
- Fractal dimension Df calculated with EBM presented good fit with results obtained with the morphological envelopes method, reaching the coefficient of determination $R^2 = 0.9176$.

Despite the fact that it is powerful, the fractal dimension method certainly needs further improvements for being used routinely. Especially a better understanding of the failure mechanisms and development of a fractal dimension damage model for fatigue life assessment seems to be applicable and will be developed by the author in further research.

Acknowledgments

The data were processed using the Mountains® software courtesy of Digital Surf, France.

Data availability statement

The data generated and/or analysed during the current study are not publicly available for legal/ethical reasons but are available from the corresponding author on reasonable request.

Appendix

Figure A1 show the subtract a surface from the extracted and leveled (LS-plane) surfaces with the color scale with histogram (in grey color) for the *Z*-axis. The differences in the location of the lowest and the highest points in the extracted and regulated areas (LS-plane) are shown in figure A2.

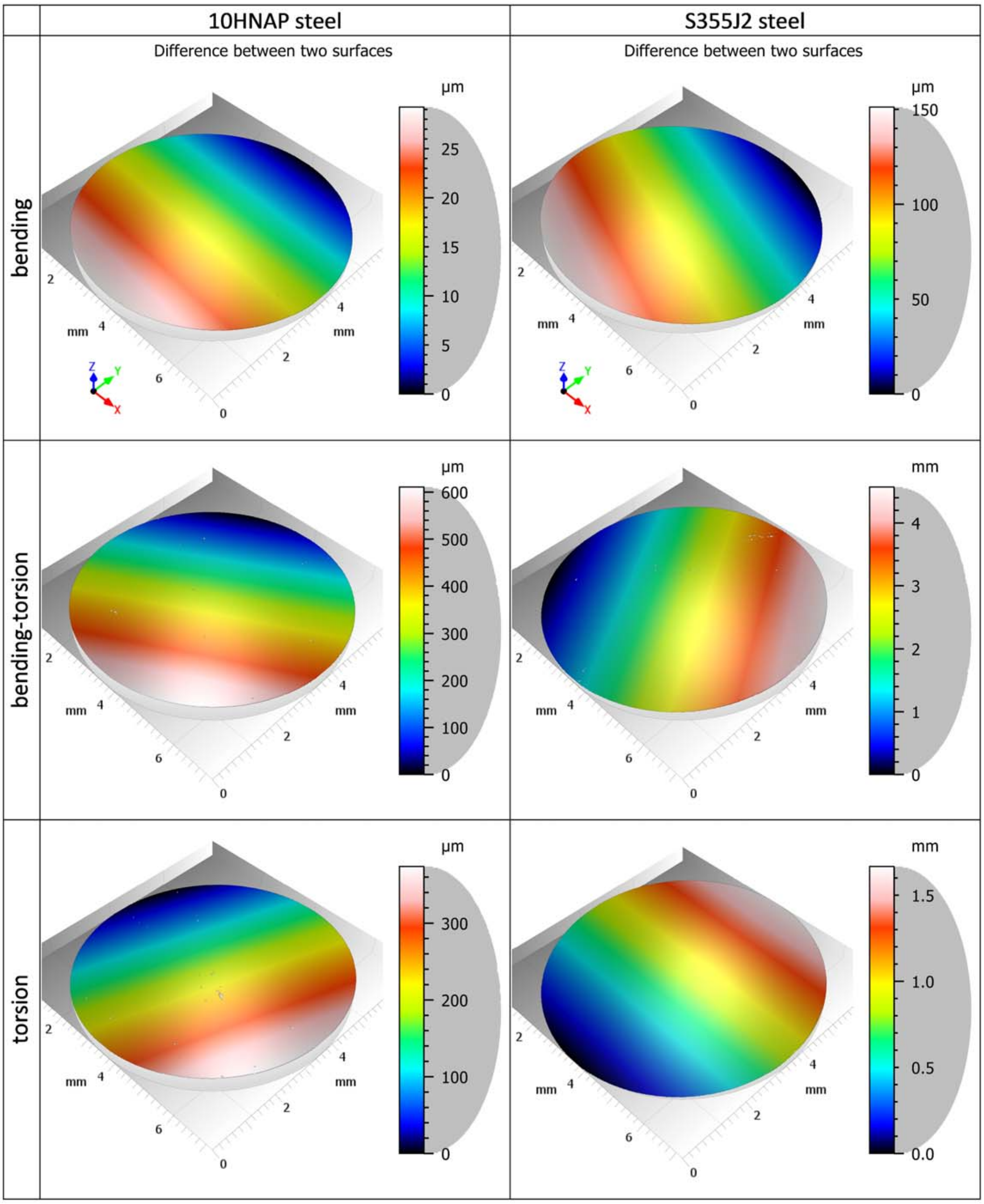

Figure A1. differences between extracted and leveled (LS-plane) surfaces.

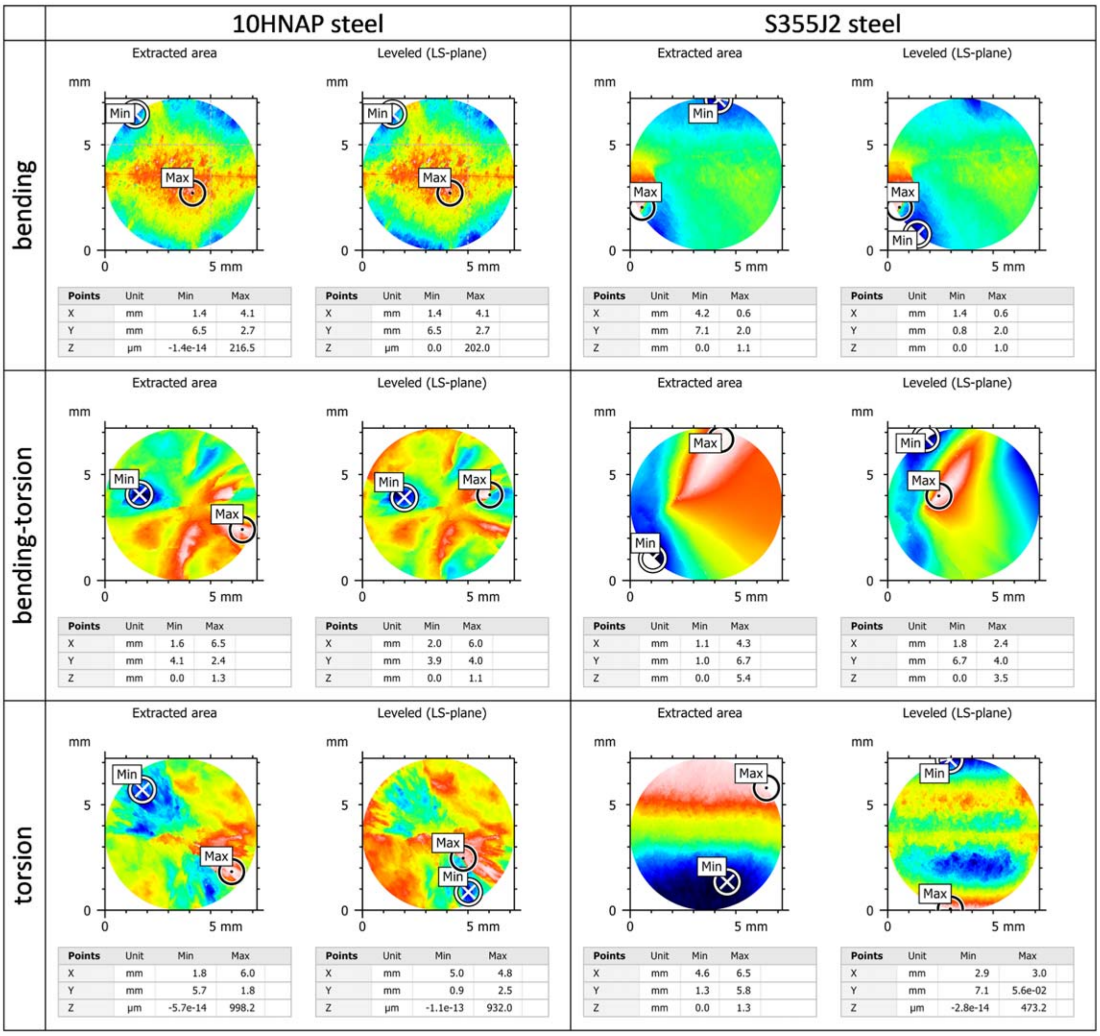

Figure A2. Differences in locations of lowest and highest points in extracted and leveled (LS-plane) surfaces.

ORCID iDs

Wojciech Macek https://orcid.org/0000-0001-9079-8877

References

[1] ISO 3274 1996 *(en), Geometrical Product Specifications (GPS) — Surface Texture: Profile Method — Nominal Characteristics of Contact (stylus) Instruments*

[2] ISO - ISO 25178-2 2012 *Geometrical Product Specifications (GPS) — Surface Texture: Areal — Part 2: Terms, Definitions and Surface Texture Parameters*

[3] ISO - ISO 16610-21 2011 *Geometrical Product Specifications (GPS) — Filtration — Part 21: Linear Profile Filters: Gaussian Filters*

[4] Podulka P 2021 The effect of surface topography feature size density and distribution on the results of a data processing and parameters calculation with a comparison of regular methods *Materials* **14** 4077

[5] Bartoszuk M 2021 Approximately model of the maximum temperature on the chip surface *Materials* **14** 2592

[6] Kaliński K J, Galewski M A, Mazur M R and Stawicka-Morawska N 2021 An experimentally aided operational virtual prototyping to obtain the best spindle speed during face milling of large-size structures *Materials* **14** 6562

[7] Płodzień M, Żyłka Ł, Sułkowicz P, Żak K and Wojciechowski S 2021 High-performance face milling of 42CrMo4 steel: influence of entering angle on the measured surface roughness, cutting force and vibration amplitude *Materials* **14** 2196

[8] Taylor M A and Bowen W P 2016 Quantum metrology and its application in biology *Physics Reports* **615** 1–59

[9] Taymanov R and Sapozhnikova K 2010 Metrological self-check and evolution of metrology *Measurement* **43** 869–77

[10] Schneller W, Leitner M, Pomberger S, Grün F, Leuders S, Pfeifer T and Jantschner O 2021 Fatigue strength assessment of additively manufactured metallic structures considering bulk and surface layer characteristics *Additive Manufacturing* **40** 101930

[11] Barnsley M F and Lésniak K 2015 On the continuity of the hutchinson operator *Symmetry* **7** 1831–40

[12] Mandelbrot B B 1982 *The Fractal Geometry of Nature* (New York: Times Books)

[13] Husain A, Reddy J, Bisht D and Sajid M 2022 Fractal dimension of India using multicore parallel processing *Computers & Geosciences* **159** 104989

[14] Mandelbrot B B, Passoja Dann E and Paullay A J 1984 Fractal character of fracture surfaces of metals *Nature* **308** 721–2

[15] Carney L R and Mecholsky J J 2013 Relationship between fracture toughness and fracture surface fractal dimension in AISI 4340 steel *Materials Sciences and Applications* **04** 258–67

[16] Akrami A, Nasiri N and Kulish V 2020 Fractal dimension analysis of Mg2Si particles of Al–15%Mg2Si composite and its relationships to mechanical properties *Results in Materials* **7** 100118

[17] Kotowski P 2006 Fractal dimension of metallic fracture surface *International Journal of Fracture* (https://doi.org/10.1007/s10704-006-8264-x)

[18] Bouchaud E, Lapasset G and Planès J 1990 Fractal dimension of fractured surfaces: a universal value? *Europhysics Letters* **13** 73

[19] Xing Y, Sun Q, Zhu M, Bai J and Wang Q 2021 Correlation between anisotropic fractal dimension of fracture surface and coercivity for Nd-Fe-B permanent magnets *Journal of Materials Research and Technology* **15** 745–53

[20] Branco R, Costa J D, Martins Ferreira J A, Capela C, Antunes F V and Macek W 2021 Multiaxial fatigue behaviour of maraging steel produced by selective laser melting *Materials and Design* **201** 109469

[21] Carpinteri A, Brighenti R and Vantadori S 2006 Surface cracks in notched round bars under cyclic tension and bending *International Journal of Fatigue* (https://doi.org/10.1016/j.ijfatigue.2005.05.006)

[22] Branco R, Prates P A, Costa J D, Borrego L P, Berto F, Kotousov A and Antunes F V 2019 Rapid assessment of multiaxial fatigue lifetime in notched components using an averaged strain energy density approach *International Journal of Fatigue* **124** 89–98

[23] Branco R, Costa J D, Berto F, Kotousov A and Antunes F V 2020 Fatigue crack initiation behaviour of notched 34CrNiMo6 steel bars under proportional bending-torsion loading *International Journal of Fatigue* **130** 105268

[24] Pawlus P, Reizer R, Wieczorowski M and Krolczyk G 2020 Material ratio curve as information on the state of surface topography—a review *Precision Engineering* **65** 240–58

[25] Slámečka K, Pokluda J, Ponížil P, Major S and Šandera P 2008 On the topography of fracture surfaces in bending-torsion fatigue *Engineering Fracture Mechanics* **75**

[26] Bies A J, Boydston C R, Taylor R P and Sereno M E 2016 Relationship between fractal dimension and spectral scaling decay rate in computer-generated fractals *Symmetry* **8** 66

[27] Podsiadlo P, Wolski M and Stachowiak G W 2015 Fractal analysis of surface topography by the directional blanket covering method *Tribology Letters* **59** 41

[28] Macek W 2019 Fractal analysis of the bending-torsion fatigue fracture of aluminium alloy *Engineering Failure Analysis* **99** 97–107

[29] Macek W, Branco R, Korpyś M and Łagoda T 2021 Fractal dimension for bending–torsion fatigue fracture characterisation *Measurement* **184** 109910

[30] Macek W 2021 Correlation between fractal dimension and areal surface parameters for fracture analysis after bending-torsion fatigue *Metals* **11** 1790

[31] Newton L, Senin N, Gomez C, Danzl R, Helmli F, Blunt L and Leach R 2019 Areal topography measurement of metal additive surfaces using focus variation microscopy *Additive Manufacturing* **25** 365–89

[32] da Conceição W S, Matos R S, Bufalino L, Ramos G Q, Zayas F G and da Fonseca Filho H D 2021 Micromorphology and fractal evaluation of Dinizia excelsa Ducke wood under three different cut conditions by atomic force microscopy *Measurement* **179** 109490

[33] Macek W *et al* 2022 Fatigue fracture morphology of AISI H13 steel obtained by additive manufacturing *International Journal of Fracture* **2022** 1–20

[34] Stępak B, Dzienny P, Franke V, Kunicki P, Gotszalk T and Antończak A 2018 Femtosecond laser-induced ripple patterns for homogenous nanostructuring of pyrolytic carbon heart valve implant *Applied Surface Science* (https://doi.org/10.1016/j.apsusc.2017.12.016)

[35] van Leer B, Genc A and Passey R 2017 Ga + and Xe + FIB milling and measurement of FIB damage in aluminum *Microscopy and Microanalysis* (https://doi.org/10.1017/S1431927617002161)

[36] Todhunter L, Leach R, Lawes S, Blateyron F and Harris P 2018 Development of mathematical reference standards for the validation of surface texture parameter calculation software *Journal of Physics: Conference Series* **1065** 082004

[37] Senin N, Thompson A and Leach R 2018 Feature-based characterisation of signature topography in laser powder bed fusion of metals *Measurement Science and Technology* **29** 045009

[38] Tălu S, Ghaderi A, Stępień K and Mwema F M 2019 Advanced micromorphology analysis of Cu/Fe NPs thin films *IOP Conference Series: Materials Science and Engineering* **611** 012016

[39] ISO 1101 2017 *Geometrical Product Specifications (GPS) — Geometrical Tolerancing — Tolerances of Form, Orientation, Location and Run-Out*

[40] Hyde J M, Cadet L, Montgomery J and Brown C A 2014 Multi-scale areal topographic analysis of surfaces created by micro-edm and functional correlations with discharge energy *Surface Topography: Metrology and Properties* **2** 045001

[41] Li J, Du Q and Sun C 2009 An improved box-counting method for image fractal dimension estimation *Pattern Recognition* (https://doi.org/10.1016/j.patcog.2009.03.001)

[42] Feng Z and Sun X 2014 Box-counting dimensions of fractal interpolation surfaces derived from fractal interpolation functions *Journal of Mathematical Analysis and Applications* **412** 416–25

[43] Zhang L, Dang F, Ding W and Zhu L 2020 Quantitative study of meso-damage process on concrete by CT technology and improved differential box counting method *Measurement: Journal of the International Measurement Confederation* **160** 107832

[44] Ţălu Ş, Stach S, Zaharieva J, Milanova M, Todorovsky D and Giovanzana S 2014 *Surface Roughness Characterization of Poly (methylmethacrylate) Films with Immobilized Eu(III) β-Diketonates by Fractal Analysis* **19** 404–21

[45] Marciniak Z, Rozumek D and Macha E 2008 Fatigue lives of 18G2A and 10HNAP steels under variable amplitude and random non-proportional bending with torsion loading *International Journal of Fatigue* (https://doi.org/10.1016/j.ijfatigue.2007.07.001)